THE JOURNAL OF PHYSICAL CHEMISTRY B

ARTICLE

pubs.acs.org/JPCB

Domain Specific Association of Small Fluorescent Probe *trans*-3-(4-Monomethylaminophenyl)-Acrylonitrile (MMAPA) with Bovine Serum Albumin (BSA) and Its Dissociation from Protein Binding Sites by Ag Nanoparticles: Spectroscopic and Molecular Docking Study

Shalini Ghosh, Sankar Jana, and Nikhil Guchhait*

Department of Chemistry, University of Calcutta, 92 A. P. C. Road, Kolkata-700009, India

ABSTRACT: Photoinduced intramolecular charge transfer produced a polar excited state in *trans*-3-(4-monomethylaminophenyl)acrylonitrile (MMAPA), rendering the resulting emission sensitive to the medium polarity. Strong binding interaction of silver nanoparticles with the probe was observed, causing fluorescence quenching through the static quenching process. The probe MMAPA was found to bind to the less polar hydrophobic, restricted proteinous environment of bovine serum albumin (BSA) resulting in the blue shift of the emission maximum with an increase in emission intensity and fluorescence anisotropy. Studies using site markers of flufenamic acid and phenylbutazone coupled with molecular docking results predicted that the binding site of the probe is in between subdomains IIIA and IB of BSA and is different from the conventional Sudlow sites. The denaturation of the probe-bound BSA by urea or heat released the probe from this proteinous environment to water marked by exactly reverse spectral changes. On the interaction of silver nanoparticles with the probe bound protein, the probe was observed to move from its binding site in the protein to the Ag^0 nanoparticle surface involving conformational changes of the protein near the probe binding site.

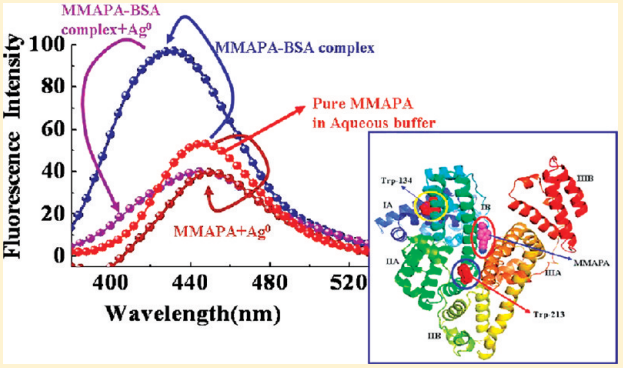

1. INTRODUCTION

Research in the field of metal nanoparticle attracts much interest today owing to special properties like their catalytic activity[1−4] and size and shape-dependent optical properties[5,6] and largely due to their promising biochemical and biological applications and antimicrobial activity.[7−10] A large area of research has been focused on the interaction of biologically relevant systems with a large variety of metal nanoparticles.[11−15] The morphological changes of a target protein on interaction with nanoparticles then are of vital interest. For the design of potential drug delivery systems based on metal nanoparticles, the biocompatibility of these particles is very important. Various techniques like surface enhanced Raman scattering (SERS), X-ray diffraction (XRD), scanning electron microscopy (SEM), transmission electron microscopy (TEM), and light scattering experiments have been used extensively to explore this field.[16−19] Silver nanoparticles can easily be prepared by wet chemical methods where the reduction of a silver salt is done with a reducing agent like sodium borohydride in the presence of a colloidal stabilizer. Sodium borohydride has been used with polyvinyl alcohol, poly(vinylpyrrolidone), BSA, citrate, and cellulose as stabilizing agents. In the case of BSA, the sulfur-, oxygen-, and nitrogen-bearing groups also mitigate the high surface energy of the nanoparticles during the reduction process.

Serum albumins are model globular proteins found abundant in plasma.[20−24] They are important transport proteins and can bind a large variety of bioactive molecules by hydrophobic, hydrophilic, and ionic interactions. BSA has three domains I, II, and III each consisting of two subdomains A and B. There are two tryptophan residues, Trp-134 and Trp-213. BSA has two abundantly reported binding sites[25] referred to as site I and site II[26,27] located in the hydrophobic cavities of subdomains IIA and IIIA, respectively. Site marker fluorescence probes can be utilized to find or guess which site a host molecule is binding to on the protein on complexation. Extensive research regarding the structure and functionality of serum albumins has been carried out by many workers.[28−30] Fluorescence probe spectroscopy is being extensively used for garnering information about the structure and dynamics of these and related proteins and their interactions with various bioactive substances.[31−40] The development and use of special polarity sensitive fluorescent probes for this purpose encompass an interesting field of research today. Photoinduced intramolecular charge transfer (ICT) from a donor to an acceptor in a molecule is known to produce dual emission in polar solvents where low energy emission are found

Received: October 1, 2011
Revised: November 24, 2011
Published: November 29, 2011

ACS Publications © 2011 American Chemical Society

to the microenvironment sensitive.[41,42] In the majority of the reports, the charge donor is the tertiary amine group. Recently, we have reported some new self-designed synthetic systems with a secondary donor which show the ICT reaction and dual emission.[43−45] Here also the charge transfer (CT) band was found to be sensitive to the polarity of the environment[45] and hence can be used as environment sensitive fluorescent probe to study the model protein, its denaturation chemically by urea and thermally, and its interaction with silver nanoparticles.

In the present case we have used *trans*-3-(4-monomethylaminophenyl)-acrylonitrile (MMAPA) as a charge transfer fluoroprobe to study protein BSA. The interaction of this small probe with BSA and its probable location inside the protein has been explored using absorption and emission spectroscopy. Site-specific binding studies using conventional site markers phenylbutazone (PB) for site I and flufenamic acid (FA) for site II and molecular docking study have been used to determine the exact binding site. The chemical and thermal denaturation process has also been tracked using the spectral response of same probe. Interestingly, the flashing out (dissociation) of probe from the protein binding site using naked Ag^0 nanoparticles and the possible morphological change of protein in the presence of Ag^0 has also been explored.

2. MATERIALS AND METHODS

2.1. Materials. The synthesis of MMAPA has been described in a previous publication.[45] BSA from Sisco Research Laboratories (SRL) was used as received. Probe−protein and probe−protein−urea/Ag^0 solutions were prepared in 0.01 M Tris-HCL buffer solution corrected to pH = 7.0 by addition of 1:1 HCl. Triply distilled water was used for preparing all solutions. Spectral grade dioxane from E-Merck was used for the micropolarity measurement.

Silver nanoparticles were prepared by reducing $AgNO_3$ in excess $NaBH_4$. Briefly, 25 mL of freshly prepared 5 mM aqueous solution of $NaBH_4$ was cooled in an ice bath. It was placed over a magnetic stirrer, and 4 mL of 2.5 mM $AgNO_3$ solution was added dropwise to it with constant stirring. The appearance of a beautiful yellow color marks the generation of the silver nanoparticles. Since a large excess of the reducing agent was taken initially, we consider the entire Ag^+ ions taken to be reduced to Ag^0. The concentration of Ag^0 in the prepared sample is determined thereby. This solution was left undisturbed for 15 min to allow the $NaBH_4$ to evaporate. The resulting solution was used as the stock silver nanoparticle solution and diluted when necessary. For every experiment, freshly prepared silver sol and protein solutions have been used to negate any problems from aggregation or denaturation. The absorption spectrum of the prepared silver sol has been checked for the typical plasmon absorption with a maximum at ∼420 nm confirming the formation of silver nanoparticles.

2.2. Steady-State Measurements. All steady-state absorption spectra were recorded on a Hitachi UV−vis U-3501 spectrophotometer, and the emission spectra were recorded on a Perkin-Elmer LS50B fluorimeter. The concentration of the CT fluorescence probe was kept at $<10^{-7}$ M for all measurements to ensure no occurrence of self-aggregation and/or self-quenching and also to maintain probe concentrations at a much lower value than the protein concentrations in all studies.

Steady-state anisotropy (r) was defined by the following relation[46]

$$r = \frac{(I_{VV} - G\cdot I_{HV})}{(I_{VV} + 2G\cdot I_{VH})} \quad (1)$$

where I_{VV} is the fluorescence intensity when both the excitation and emission polarizers are oriented vertically and I_{VH} is the fluorescence intensity when the excitation polarizer is vertically oriented and the emission polarizer is horizontally oriented. The factor G is defined as

$$G = \frac{I_{HV}}{I_{HH}} \quad (2)$$

I_{HV} is the fluorescence intensity with the excitation polarizer horizontally and the emission polarizer vertically oriented, and I_{HH} is the fluorescence intensity with both the excitation and the emission polarizers oriented horizontally.

2.3. Molecular Docking. The Protein Data Bank (PDB) structure of BSA generated using the Swiss-model server[47] was used for docking studies. The human serum albumin (HSA) structure (PDB ID 1AO6)[48] is served as a template in building the structural model for BSA. Only one gap is present in the pairwise sequence over all of the residues of the BSA sequence. The 75% identity and 87% similarity is shared between HSA and BSA sequences.[49] This model for BSA was hence reliable and most likely resembles to the native three-dimensional structure. MMAPA structure optimization was performed by the Gaussian 03[50] software using the Hartree−Fock (HF) method and 6-31++G (d,p) basis set. This optimized structure was used to generate the PDB structure of the probe and then used for the docking studies.

Molecular docking was performed to obtain the binding energy of the protein−probe complex, and the binding sites were then analyzed. The docking experiments were performed using the docking software AutoDock4.2[51] along with the AutoDock Tools (ADT). AutoDock generates different ligand conformers using a Lamarkian genetic algorithm (LGA). The GA is implemented with an adaptive local method search. The energy based Autodock scoring function includes terms accounting for short-range van der Waals and electrostatic interactions, loss of entropy upon ligand binding, hydrogen bonding, and solvation. For the recognition of the binding sites in BSA, docking was carried out with setting of grid size to 126, 102, and 126 along x, y, and z axes with a grid spacing of 0.452 Å after assigning the protein and probe with Kollman charges. The grid center was set at 0.026, 0.108, and 0.114 Å. Initially, AutoGrid was run to generate the grid map of various atoms of the ligand and receptor. After the completion of the grid map AutoDock was run by using autodock parameters as GA population size: 500 and maximum numbers of energy evaluations: 2.5×10^7 with numbers of generations: 27 000. A total of 100 runs[52] were carried out. From them the 10 minimum energy conformers were picked out in order of their rank and score.[53,54] The root-mean-square cluster tolerance was set to 2.0 Å[54] in each run.

2.4. Scanning Electron Microscope Imaging. The scanning electron micrographs were taken using a scanning electron microscope (SEM), Hitachi S3400N, Japan, with SE mode applying an accelerating voltage of 15 kV. The test solution drops were placed on a 5 × 5 × 1 mm glass slide and were dried in vacuum and left overnight before SEM imaging. The prepared samples were placed on sample studs and coated with gold by ion sputtering.

2.5. Circular Dichroism Measurements. The CD spectra of aqueous buffer solutions of BSA at various Ag^0 concentrations

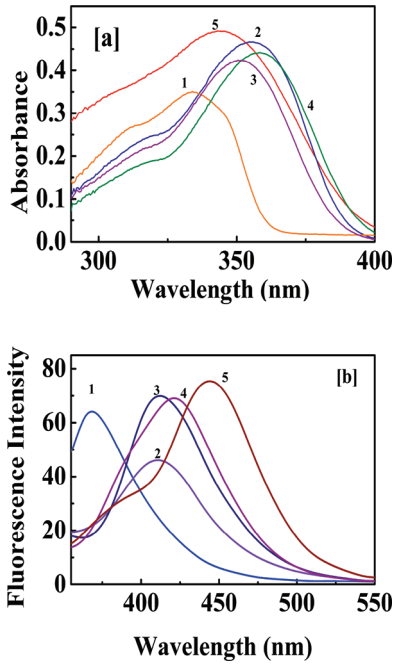

Figure 1. Room temperature (a) absorption and (b) emission spectra (excitation at corresponding absorption maxima) of MMAPA in: (1) cyclohexane, (2) tetrahydrofuran, (3) acetonitrile, (4) ethanol, and (5) water.

were recorded by using a quartz cuvette of 1 mm path length with a Jasco J-815 CD spectrophotometer at room temperature. The BSA concentration was maintained at 10 μM. The mean residual ellipticities (MRE) or molar ellipticities at 208 nm were calculated using the following relation

$$[\Theta]_{208} = \frac{\Theta_{obs}}{10nlC_p} \quad (3)$$

where Θ_{obs} is the CD in millidegrees at 208 nm, n is the number of residues in the protein, l is the path length of the cell, and C_p is the protein concentration in moles dm^{-1}. The percentage of α-helix content was calculated from the MREs using the relation

$$\%\alpha - \text{helix} = \frac{-([\Theta]_{208} - 4000)}{33000 - 4000} \times 100 \quad (4)$$

3. RESULTS AND DISCUSSION

3.1. Spectral Characteristics of MMAPA. Except for a very slight dependence on the hydrogen bonding ability of the solvents, the absorption spectra of MMAPA in all solvents are almost independent of solvent polarity and are comprised of a strong $S_0 \rightarrow S_1$ transition band at ~350 nm and a weaker $S_0 \rightarrow S_2$ transition at ~318 nm as seen in Figure 1a.[45] The emission characteristics of MMAPA are however very sensitive to solvent polarity (Figure 1b). Photoinduced intramolecular charge transfer from the secondary amine donor to the nitrile acceptor is found to produce dual emission in polar solvents like methanol and water.[45] The red-shifted stronger emission band was assigned to the charge transfer (CT) emission. Obvious stabilization of this polar excited CT state in more polar solvents was found to produce a red-shift of the CT maximum in progressively

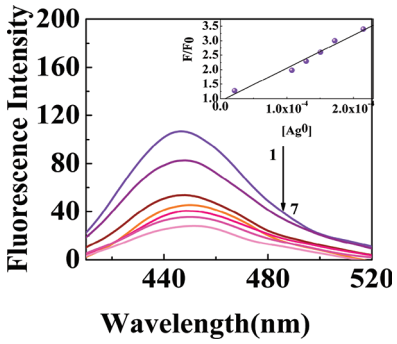

Figure 2. Quenching of MMAPA fluorescence (λ_{ex} = 350 nm) on addition of Ag^0 (1, 0 μM; 2, 21.5 μM; 3, 107.5 μM; 4, 129 μM; 5, 150.5 μM; 6, 172 μM; 7, 215 μM Ag^0 concentrations). Inset: Stern–Volmer plot for Ag^0 induced quenching of MMAPA fluorescence.

polar solvents. This sensitivity of the CT band position toward the polarity of the fluorophore environment has been further used for monitoring the model protein BSA, its chemical and thermal denaturation, and its interaction with Ag^0.

3.2. Interaction of MMAPA with Ag^0. The steady state emission of MMAPA was found to be quenched on interacting with the silver nanoparticles as shown in Figure 2. The Stern–Volmer plot[55] for quenching (Figure 2 inset) was found to be linear, suggesting either a purely static or purely dynamic mechanism is operative. Time-resolved emission measurements showed no change in the fluorescence lifetime of the probe in the presence of Ag^0 which rules out the possibility of dynamic quenching. The Stern–Volmer quenching constant was found to be 1.13×10^4 L mol^{-1}. The number of binding sites and the binding constant were calculated from the Scatchard plot[55] and found to be 1.48 and 6.32×10^5 L mol^{-1}, respectively. The observed quenching is in all probability due to the attachment of the MMAPA molecule on the Ag^0 surface via the lone pair on the amine group. The ICT process should be stopped due to the unavailability of the lone pair, and hence the emission is quenched. Similar quenching of the ICT emission in *trans*-2-[4-(dimethylamino)styryl]benzothiazole has been reported and explained likewise by Das et al. recently.[56]

3.3. Binding of MMAPA with BSA. The introduction of MMAPA into buffer solutions of progressively higher BSA concentration is marked by the blue-shift of the polarity sensitive red-sided CT band maximum and a simultaneous increase in intensity (Figure 3a). This blue-shift indicates a pronounced lowering of the surrounding environment polarity due to movement of the probe into the much less polar proteinous environment which destabilizes the polar CT state. In the proteinous hydrophobic environment the nonradiative decay channels active in water are also deactivated and hence the observed increase in the emission intensity. The Benesi–Hildebrand plot[57] (plot of $1/(I - I_0)$ against $1/[\text{BSA}]$, I = emission intensity of protein bound probe, I_0 = emission intensity of the free probe) for the 1:1 association of the probe with the model protein as seen in Figure 3a (inset) is found to be linear throughout. This observed linearity proves the 1:1 stoichiometry of binding between the probe and BSA and the association constant and free-energy change for this binding process calculated from this plot are 5.01×10^4 L·mol^{-1} and −6.38 kcal mol^{-1}, respectively. The negative value of free energy change indicates a spontaneous complexation reaction.

dx.doi.org/10.1021/jp2094752 |J. Phys. Chem. B 2012, 116, 1155–1163

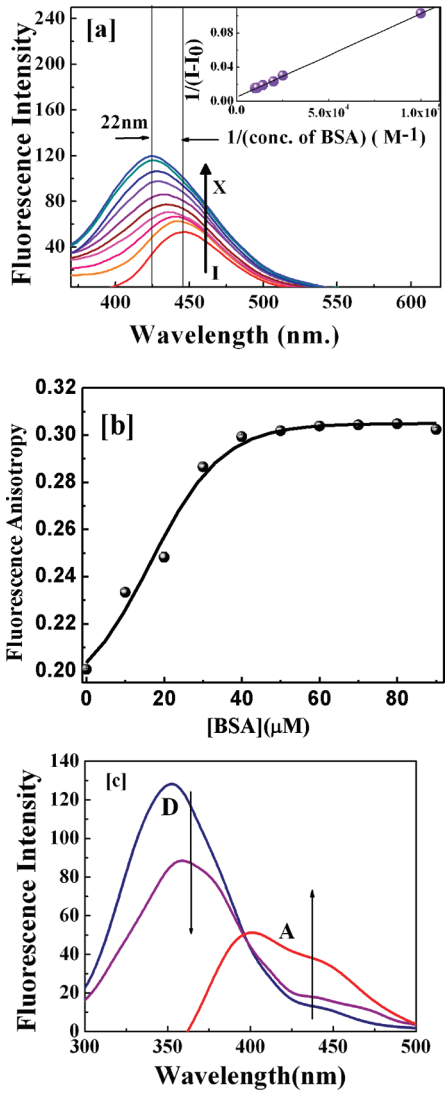

Figure 3. (a) Emission spectra of MMAPA (λ_{ex} = 350 nm) in (I) 0 μM, (II) 10 μM, (III) 20 μM, (IV) 30 μM, (V) 40 μM, (VI) 50 μM, (VII) 60 μM, (VIII) 70 μM, (IX) 80 μM, and (X) 90 μM BSA solutions in 0.01 M tris-HCl buffer, pH = 7.0. Inset: Benesi−Hildebrand plot for 1:1 complexation of MMAPA to BSA. (b) Variation of fluorescence anisotropy of MMAPA with increasing BSA concentrations. (The data points here are the ± standard errors (SE) of six independent measurements.) (c) Flourescence energy transfer between donor tryptophan (D) and acceptor MMAPA (A). Clear quenching of donor emission and growth of acceptor emission is observed. (Arrow indicates increasing MMAPA additions.)

The rigid proteinous environment in fact does restrict the motional freedom of the probe which is reflected in the increase fluorescence anisotropy of MMAPA at higher BSA concentrations.[50] In rigid surroundings, the rotational diffusion of a fluorophore is largely arrested leading to less extent of depolarization of its emission and hence greater anisotropy. Fluorescence anisotropy serves as a sensitive tool for monitoring changes in the motional freedom of a fluorophore on introduction into rigid, microheterogeneous media like a protein or a micelle interior. As seen in Figure 3b, with increasing BSA concentrations, there is indeed a steady rise of fluorescence anisotropy, and it levels off after 50 μM BSA marking the movement of the fluorophore from a free water environment to a rigid proteinous environment on binding to BSA.

3.3.1. Fluorescent Resonant Energy Transfer. Figure 3c outlines the fluorescence resonant energy transfer (FRET) from the tryptophan residue of BSA to probe MMAPA. Three conditions need to be fulfilled for FRET to take place from a prospective donor to a suitable acceptor: (i) there needs to be substantial overlap between the emission characteristics of the donor and the absorption of the acceptor, (ii) the donor and acceptor transmission dipoles need to have proper orientations, and (iii) the distance between the donor and the acceptor needs to be optimal. It is found that there is good overlap between the absorption spectrum of MMAPA with emission of tryptophan of BSA. As seen in Figure 3c, on exciting the protein near the tryptophan absorption at 290 nm (where there is no MMAPA absorption) the Trp emission is quenched with gradual addition of the probe. A simultaneous generation and increase of the protein bound probe emission is observed at ∼440 nm which can only be possible if FRET takes place from the excited tryptophan of BSA to the bound probe MMAPA which absorbs at the emission of the tryptophan residues. This explains the quenching of the tryptophanyl fluorescence and growth of the probe emission.

Fluorescence resonant energy transfer efficiency can be calculated by the following equation[50]

$$E = 1 - \frac{F}{F_0} = \frac{{R_0}^6}{r^6 + {R_0}^6} \tag{5}$$

where E = efficiency of energy transfer, F = fluorescence intensity of MAPAME when bound to BSA, F_0 = fluorescence intensity of MAPAME in the absence of BSA, r is the distance between the donor and the acceptor, and R_0 is the critical distance at which the extent of energy transfer is 50%. The energy transfer efficiency (E) for FRET between donor Trp of BSA and acceptor MAPAME has been calculated to be 96%. The value for R_0 could be calculated using the following equation

$$R_0 = 8.74 \times 10^{-25} K^2 n^{-4} \Phi J \tag{6}$$

where K^2 is the spatial factor of orientation (= 2/3), n is refractive index of the medium (= 1.33), Φ is the fluorescence quantum yield of the donor (= 0.15), and J is the overlap integral between donor emission and acceptor absorption defined as

$$J = \frac{\int_0^\infty F(\lambda)\varepsilon(\lambda)\lambda^4 \, d\lambda}{\int_0^\infty F(\lambda) \, d\lambda} \tag{7}$$

Here $F(\lambda)$ is the fluorescence of the donor in the wavelength range λ and λ+dλ, and $\varepsilon(\lambda)$ is the molar extinction coefficient of the acceptor at the wavelength λ. Using this equation the value of J was calculated, and then the values for R_0 and r were calculated to be 2.51 nm and 1.85 nm, respectively. It is well-known that for good FRET the donor and acceptor should lie within a distance of 2−8 nm between them and the condition $0.5R_0 < r < 1.5R_0$ should be fulfilled. Both these conditions are in fact satisfied well for BSA-bound MAPAME[58,59] as is also supported by the molecular docking results.

3.3.2. Molecular Docking Analysis. From the docking calculation, the conformer with minimum binding energy is picked up from the 10 minimum energy conformers from the 100 runs[53,54]

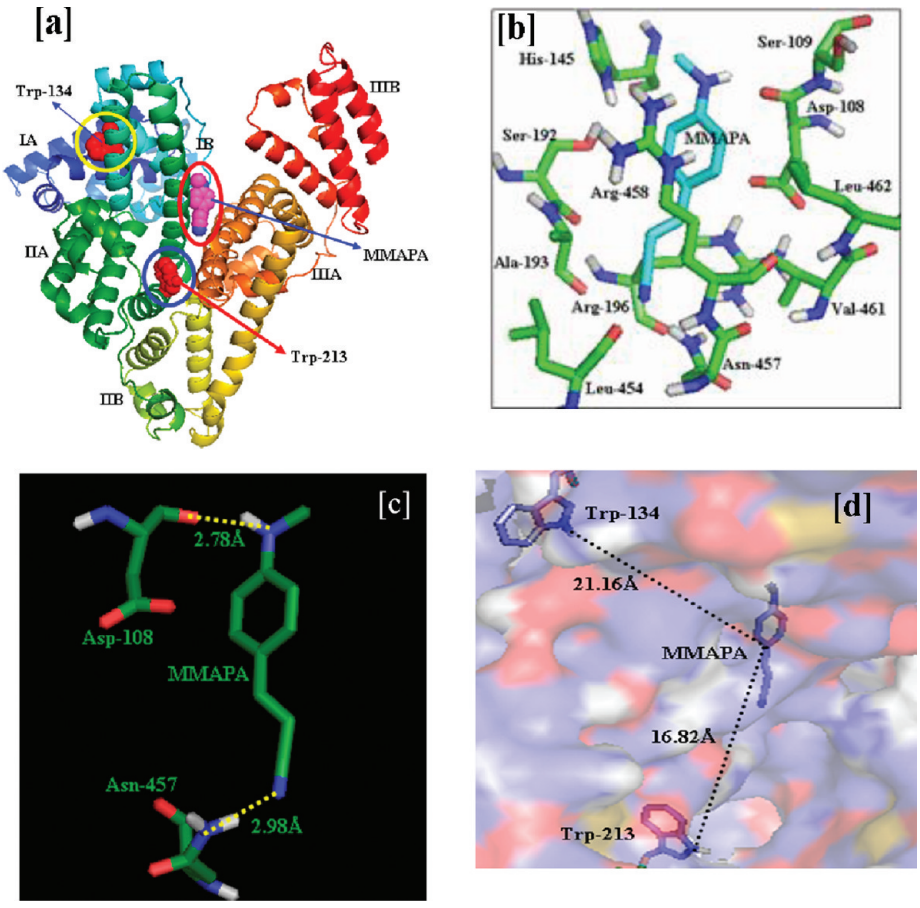

Figure 4. Molecular docking analysis results: (a) minimum energy dockimg configuration showing all subdomains of BSA, Trp-134, Trp-213, and bound MMAPA (BSA is shown in ribbon structure, two tryptophans and bound probe represented by the sphere model); (b) hydrophilic and hydrophobic amino acid residues surrounding bound MMAPA; (c) two hydrogen-bonding interactions between Asp-108, Asn-457, and bound MMAPA, and (d) distance between bound MMAPA and Trp-134 and Trp-213 in minimum energy docking pose presented by stick model using PYMOL.

and is shown in the Figure 4a. The run data for the conformers are listed in Table 1. MMAPA binds deep within the pocket between the subdomains IB and IIIA in the minimum energy conformer. As seen in Figure 4b, the probe molecule is surrounded by the hydrophobic side chains and also the positively charge residues, namely, Ala-193, Leu-454, Val-461, Leu-462 and His-145, Arg-196, Arg-458 respectively, and so forth. It was hence inferred that the interaction between two species, that is, MMAPA and BSA is mainly hydrophobic in nature. Hydrogen bonding and electrostatic interactions were also present due to the presence of several ionic and polar groups near the probe. Within a distance of 2.6−3.5 Å[53−55] between donor and acceptor atoms we have considered two hydrogen bonds one between the nitrile group of MMAPA and the adjacent N atom of Asn-457 (2.98 Å) and another between the amine group of MMAPA and the adjacent O atom of Asp-108 (2.78 Å) (Figure 4c). This hydrogen bonding supports a decrease in hydrophilicity instead of increasing hydrophobicity within the complex of protein BSA and probe MMAPA. From the docking simulation the observed free energy change of binding (ΔG) for the complex BSA + MMAPA is calculated to be −5.30 kcal mol^{-1} is slightly lower than the experimental free energy of binding (−6.38 kcal mol^{-1}) obtained from the Benesi−Hildebrand plot. This apparent mismatch in the free energy changes could be due to the exclusion of the solvent and/or rigidity of some other receptor besides tryptophan in the molecular docking studies. The distance between tryptophan and the bound probe obtained from the FRET studies (1.85 ± 0.01 nm) is also comparable with the distances obtained from docking simulation where the

Table 1. Docking Results of BSA and MMAPA by Using the AutoDock Program Generated Different Ligand Conformers Using Lamarkian Genetic Algorithm

rank	run	binding energy (kcal M^{-1})	$^{a}K_i$ (mM)	cluster rmsd	reference rmsd
1	70	−5.30	0.130	0.00	6.88
2	41	−4.73	0.339	0.00	31.44
3	25	−4.17	0.871	0.00	7.71
4	6	−3.97	1.22	0.00	8.78
5	61	−3.94	1.30	0.00	13.76
6	66	−3.85	1.52	0.00	9.71
7	62	−3.78	1.69	0.00	14.50
8	48	−3.74	1.81	0.00	29.87
9	85	−3.67	2.02	0.00	19.46
10	77	−3.65	2.10	0.00	6.65

$^{a}K_i$ is the inhibition constant.

dx.doi.org/10.1021/jp2094752 |J. Phys. Chem. B 2012, 116, 1155–1163

Table 2. Effect of Site Markers Phenylbutazone (PB) and Flufenamic Acid (FA) on the Binding of Probe MMAPA with Protein BSA

	no. binding sites	binding constant of MMAPA to BSA
pure BSA	1.06	6.3×10^4 L mol^{-1}
BSA-PB	1.04	6.02×10^4 L mol^{-1}
BSA-FA	1.09	11.48×10^4 L mol^{-1}

distances of the probe are 1.68 ± 0.02 nm and 2.11 ± 0.01 nm from Trp-213 and Trp-134, respectively (Figure 4d). The docking results also support movement of the probe from the more polar hydrophilic region to the much less polar hydrophobic region and consequent emission intensity enhancement.

3.3.3. Effect of Site-Markers on the Binding of MMAPA to BSA. The site markers phenylbutazone (PB) for site I and flufenamic acid (FA) for site II were employed to locate the probable binding site for MMAPA in BSA. It is found that the fluorescence intensity of BSA, BSA-PB, and BSA-FA on excitation at 295 nm was quenched by the addition of MMAPA. The binding constant and number of binding sites of MMAPA to BSA in each case was calculated using the double logarithmic plot and are listed in Table 2. For all cases a single binding site is expected from the results. The binding constant for pure BSA with probe obtained this way is 6.3×10^4 L mol^{-1} which is comparable to that obtained from the B−H plot (5.01×10^4 L mol^{-1}). In presence of phenylbutazone the binding constant remains almost unchanged at 6.02×10^4 L mol^{-1}, suggesting out of doubt that MMAPA does not bind at the Sudlow site I. The binding constant of MMAPA to BSA in the presence of the site II marker flufenamic acid shows an unexpected increase from that with pure BSA. The value of K for binding to BSA in the presence of FA is found to be 11.48×10^4 L mol^{-1} which is almost double that of with pure BSA. This unexpected trend can well describe and support the result of the molecular docking studies. The binding of our probe to BSA is enhanced in presence of flufenamic acid, that is, when the site II in subdomain IIIA is occupied by the site marker. MMAPA hence definitely does not bind in site II or else a decrease in binding constant would have been observed. However, experimental results indicate that it must bind in a position which is affected by the presence of the site II marker FA. The binding of any molecule to a protein in a definite subdomain is bound to produce some structural/conformational changes in the surrounding environment. According to the molecular docking results, MMAPA binds in the cleft between subdomains IB and IIIA and not at any of the established binding sites. This position is far away from the subdomain IIA, and hence the indifference to the presence of the site I marker is explained. Binding so close to the subdomain IIIA and yet not at site II could explain the increase in binding constant in the presence of the site II marker. When flufenamic acid binds to BSA in subdomain IIIA, it could trigger changes in protein conformation near its binding site such that binding of another molecule like MMAPA near this area would in fact become easier. This can explain the apparent increase in binding constant of MMAPA to BSA already marked with FA. The results of site marker studies and molecular docking are mutually compatible and propose a binding site for our probe on BSA hitherto very less explored.

3.3.4. Effect of Urea. The addition of urea to a solution of MMAPA bound to BSA is expected to denature the protein,[60,61]

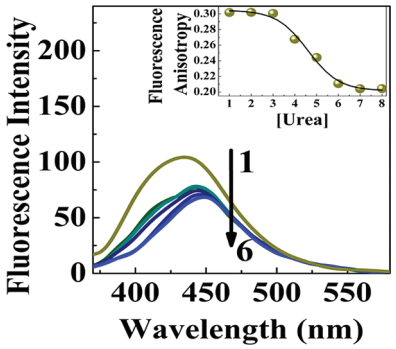

Figure 5. Variation of emission spectra (λ_{ex} = 350 nm) of MMAPA in 50 μM BSA with increasing urea concentration (1, 0 M; 2, 2 M; 3, 3 M; 4, 4 M; 5, 7 M; and 6, 8 M urea); Inset: Variation of fluorescence anisotropy of BSA-bound MMAPA (in 50 μM BSA) with increasing urea concentration.

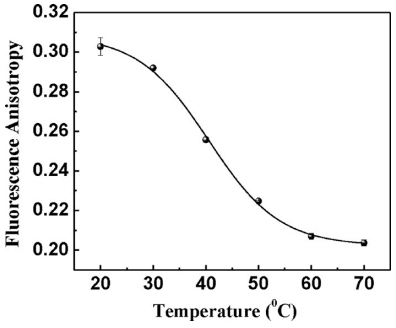

Figure 6. Variation of fluorescence anisotropy of MMAPA in 50 μM BSA with increasing temperature.

and the bound probe will show spectral changes in track with the alterations of the micropolarity of its environment owing to this. Urea being a chaotrope should also disrupt the hydrophobic interactions that are most responsible for the probe binding as was evident from the docking studies. As seen in Figure 5, the ICT emission maxima of the protein bound probe undergoes a red-shift in the presence of urea, and in high urea concentrations ([urea] = 8 M) the position of this band is the same as that in water. This suggests a movement of the probe back to the polar water phase from the proteinous less polar environment by chemical denaturation with the addition of urea. Gradually being freed into the water environment due to chemical denaturation, the motional restriction on the probe in the protein environment steadily decreases, and this is indeed reflected in the fluorescence anisotropy changes. As in Figure 5 (inset), on increasing urea concentrations the anisotropy of the protein bound MMAPA decreases steadily, and in high concentrations of urea ([urea] = 8 M) the anisotropy (= 0.204) is very close to the anisotropy of the fluorophore in free water (= 0.200). This indicates almost complete denaturation of BSA at such high urea concentrations and matches with the multitude of reports on urea-induced denaturation of BSA.[29,30,35,36]

3.3.5. Effect of Temperature. BSA is also denatured thermally at and above 60 °C, and we have also attempted to follow this thermal denaturation process by using probe MMAPA and its special spectral properties. As in the case of chemical denaturation, increasing the temperature produces similar changes in anisotropy of the BSA bound MMAPA (Figure 6). A steady decrease in anisotropy is observed with increasing temperatures

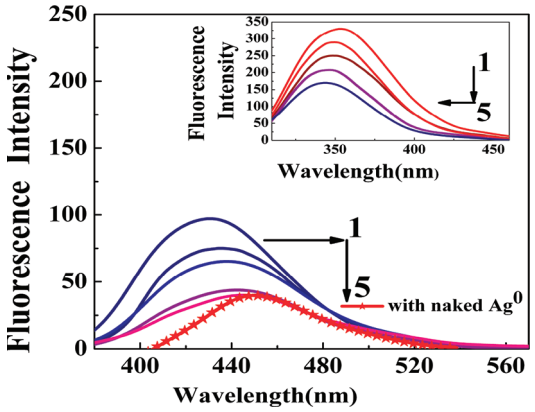

Figure 7. Effect of Ag^0 on the emission spectrum of MMAPA in 80 μM BSA (λ_{ex} = 350 nm). Inset: Effect of Ag^0 on the tryptophan emission of BSA (1) 0 μM, (2) 8.6 μM, (3) 17.24 μM, (4) 34.48 μM, and (5) 51.72 μM Ag^0) (λ_{ex} = 290 nm).

and at high temperatures the anisotropy of the probe (= 0.204) is very near that observed in pure water at room temperature. This is indeed indicative of complete denaturation at this temperature and release of the probe back to the water phase owing to this.

3.4. Interaction of MMAPA Bound BSA with Silver Nanoparticles. Figure 7 shows the variation of emission of BSA bound probe MMAPA with the addition of higher concentrations of silver nanoparticles. A clear red shift of the emission maximum is observed with a concomitant decrease in intensity as more silver nanoparticles are introduced in the system. The final emission spectrum corresponds very well with the quenched emission of MMAPA in the presence of naked silver nanoparticles at the same NP concentration. This is suggestive of substantial conformational change of the protein which releases the attached probe to the Ag^0 surface. Although the observed changes are much like those observed for denaturation of the probe bound protein, subsequent SEM, CD, and acrylamide-induced quenching studies show that the interaction of BSA with the silver nanoparticles does not denature the protein. Instead a probable conformational change is more feasible. Conformational changes of the protein by adsorption on the Ag^0 surface is also evident from the gradual blue shift of the tryptophanyl fluorescence of the protein with increasing silver nanoparticle concentrations as shown in Figure 7 (inset). Denaturation (like that by urea) should have produced a red-shift of the tryptophanyl emission.[61] The observed blue-shift is suggestive of some conformational change which releases the bound probe to the silver NP but does not expose the tryptophan residues to the bulk water. Instead the tryptophan residues sense a more hydrophobic environment which is signaled by the blue-shift.

3.4.1. Acrylamide Quenching Studies. Quenching of tryptophan fluorescence of BSA in the presence and absence of silver NP corroborates the possible structural changes of the protein. Quenching by acrylamide (AA) depends to a large extent on the accessibility of the tryptophan residues to the quencher.[61] For both the pure protein and the Ag^0-interacted protein the Stern–Volmer plots for tryptophanyl fluorescence quenching by AA are found to be linear (Figure 8). However, in the presence of Ag^0, the K_{SV} value for AA induced quenching is lower (6.87 M^{-1}) than that for pure BSA (9.7 M^{-1}). A lower extent of quenching hints to the lesser accessibility of the tryptophan residues. This can be possible if BSA undergoes a slight structural change on

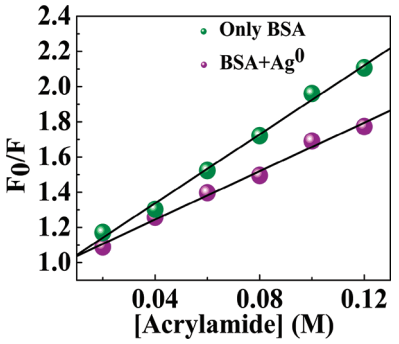

Figure 8. Quenching of intrinsic tryptophan fluorescence of BSA with acrylamide in the absence and presence of Ag^0 (21.5 μM) (λ_{ex} = 290 nm).

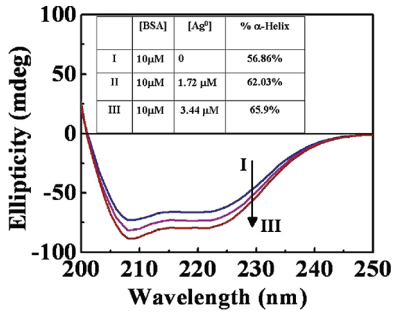

Figure 9. Far-UV CD spectra of 10 μM BSA in (I) absence of, (II) 1.72 μM, and (III) 3.44 μM Ag^0 nanoparticle.

interaction with the NP which leads to lesser exposure of the tryptophan residues. The observed blue-shift of the tryptophan fluorescence on interacting with Ag^0 is well in keeping with this assumption. Interaction with silver NP produces such conformational change in BSA which makes the tryptophan residues less exposed, probably moving them to a less polar environment accounting for the blue-shift as well as the reduced the extent of AA induced quenching. The denaturation of BSA would in fact have produced opposite results as a larger exposure of tryptophan to external quenchers would then be expected.

3.4.2. Circular Dichroism Studies. The far-UV CD studies hint at a possible stabilization of the secondary structure of BSA on interacting with silver NP. The CD spectra recorded from 200 to 250 nm show the two characteristic bands for BSA at 208 and 222 nm (Figure 9). On addition of Ag^0 both bands show gain in negative intensity, hinting at a more stable secondary structure.[62] The α-helical content increases from 56.86% for pure BSA to 65.9% in the presence of 3.44 μM Ag^0. This is consistent with all of the experimental results so far discussed. Interaction of protein with Ag^0 does not denature the protein which would in fact disrupt the helicity but instead produces a stabilizing effect on the secondary structure.

3.4.3. Scanning Electron Microscope Imaging. The SEM images for the naked silver nanoparticles, buffer BSA, and BSA adsorbed on Ag^0 are shown in Figure 10a, b, and c, respectively. BSA spreads over the nanoparticle surface leading to the stabilization of the silver colloid. From the micrographs it is clear that the silver nanoparticles are completely coated with the protein, and in this state the globular form of the albumin is not lost, suggesting out of doubt that interaction with silver nanoparticles does in no way denature this protein.[63]

dx.doi.org/10.1021/jp2094752 |J. Phys. Chem. B 2012, 116, 1155–1163

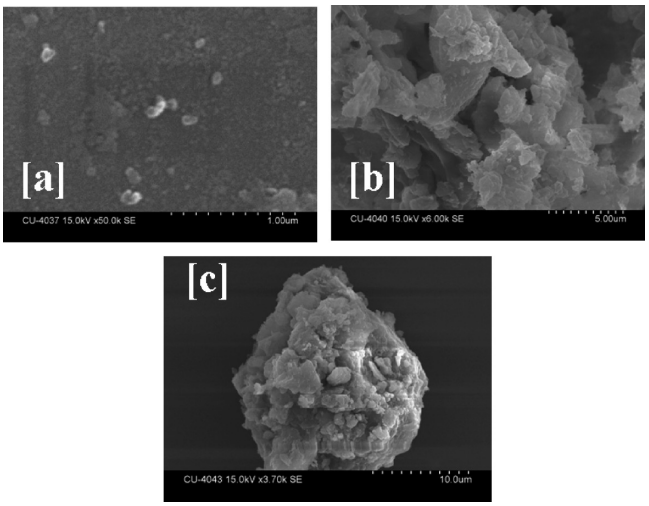

Figure 10. Scanning electron microscope images of [a] only silver NP, [b] only BSA, and [c] BSA (80 μM) + silver NP (51.72 μM).

4. DISCUSSION

The interaction of MMAPA with BSA moves it to a less polar, more hydrophobic, rigid proteinous environment as is evident from the blue-shift and increase in intensity of the polarity sensitive CT maximum and simultaneous rise in fluorescence anisotropy. Molecular docking studies coupled with site marker studies indicate possible binding of MMAPA in between subdomains IIIA and IB of BSA. Any changes induced in these subdomains after binding would produce alterations in the spectral response of the bound probe. Denaturation by urea or heat unfolds the protein exposing both the bound probe and the tryptophan residues to the more polar bulk aqueous environment. Both the probe fluorescence and the intrinsic tryptophanyl fluorescence show red-shifts. Release into the free environment also relaxes the motional restrictions on the bound probe, producing a decrease in fluorescence anisotropy. The fluorophore MMAPA undergoes static quenching of its CT emission on interacting with silver nanoparticles suggesting formation of a ground state complex. When the protein interacts with Ag^0, the protein spreads on the nanoparticle surface covering it completely as is evident from the SEM micrographs. This is accompanied by some structural changes in the protein which releases the bound probe to the NP surface. The greater affinity of the probe toward the Ag^0 surface than the BSA binding site is somewhat justified by the difference in the respective association constants. The association constant values for the BSA-probe pair and the Ag^0-probe pair are 5.01×10^4 L mol^{-1} (from the B−H plot) and 6.32×10^5 L mol^{-1}, respectively. The release of the probe could account for the observed red-shift of the emission maximum of bound MMAPA. The tryptophanyl fluorescence of BSA however undergoes a slight blue-shift. All of these results together suggest that on the interaction of BSA with Ag^0 definite structural changes occur in the subdomains IB and IIIA between which the probe binds, whereas much lesser changes are hinted in subdomains IA and IIB containing the tryptophan residues which lead to them being less exposed now. Lower exposure of the tryptophan residues are also marked by the lesser extents of quenching of their fluorescence by acrylamide for Ag^0 interacted BSA than for native BSA. Far-UV CD spectra confirm no loss of hellicity of BSA on interaction with Ag^0. Instead a more stable secondary structure results. MMAPA is thus established as a robust yet fine probe for marking domain specific changes in BSA structure when it interacts with silver nanoparticles and hence for studying the biocompatibilty of this and similar metal-nanoparticles.

5. CONCLUSION

The polarity sensitive charge transfer emission band of MMAPA has been utilized as a probe for the study of model biological system BSA and its denaturation by urea and also thermally. Binding of the probe to BSA is marked by blue-shift of ICT band maximum and an increase in fluorescence intensity and anisotropy. Site specific binding studies involving site I and II markers coupled with molecular docking analysis suggest binding of MMAPA between subdomains IB and IIIA in BSA. The spectral response of the protein bound probe on interacting with silver nanoparticles hint at a dissociation of the bound probe from the protein binding site. Further analysis clearly hints at larger structural changes of BSA in the subdomains IB and IIIA between which the probe binds, whereas much lesser changes are hinted in subdomains IA and IIB containing the tryptophan residues which lead to them being less exposed now. The denaturation of protein does not take place on interaction with the NP. Instead, according to the CD results, the secondary structure of BSA is stabilized, and no loss in hellicity is registered.

AUTHOR INFORMATION

Corresponding Author

*Tel.: 91-33-2350-8386. Fax: +91-33-2351-9755. E-mail: nguchhait@yahoo.com.

ACKNOWLEDGMENT

This work is supported by DST, India (Project No. SR/S1/PC/26/2008). S.G. thanks DST for a fellowship from the above project. The authors would like to thank Dr. P. K. Maity and Amit Mallik, Department of Chemical Technology, University of Calcutta for SEM measurement.

REFERENCES

(1) Lu, Y.; Mei, Y.; Drechsler, M.; Ballauff., M. *Angew. Chem.* **2006**, *45*, 813–816.
(2) Run, X.; Dingsheng, W.; Jiatao, Z.; Yadong, L. *Chem. Asian J.* **2006**, *1*, 888–893.
(3) Xin, G.; Tao, L.; Jun, Z.; Xinjian, L.; Genxi, L. *ChemBioChem* **2004**, *5*, 1686–1691.
(4) Narayanan, R.; El-Sayed, M. A. *Nano Lett.* **2004**, *4*, 1343–1348.
(5) Emory, S. R.; Nie, S. *J. Phys. Chem. B* **1998**, *102*, 493–497.
(6) Haes, A. J.; Van Duyne, R. P. *J. Am. Chem. Soc.* **2002**, *124*, 10596–10604.
(7) Sondia, I.; Salopek-Sondib, B. *J. Colloid Interface Sci.* **2004**, *275*, 177–180.
(8) Kim, J. S.; Kuk, E.; Yu, K. N.; Kim, J.-H.; Park, S. J.; Lee, H. J.; Kim, S. H.; Park, Y. K.; Park, Y. H.; Hwang, Kim, Y. K.; et al. *Nanomed.: Nanotechnol., Biol. Med.* **2007**, *3*, 95–100.
(9) Sharma, V. K.; Yngarda, R. A.; Lin, Y. *Adv. Colloid Interface Sci.* **2009**, *145*, 83–96.
(10) Panáek, A.; Kvítek, L.; Prucek, R.; Kolář, M.; Veeřová, R.; Pizúrová, N.; Sharma, V. K.; Nevěná, T.; Zbořil, R. *J. Phys. Chem. B* **2006**, *110*, 16248–16253.
(11) Lee, K. J.; Nallathamby, P. D.; Browning, L. M.; Osgood, C. J.; Xu, X.-H. N. *ACS Nano* **2007**, *1*, 133–143.

(12) Malinsky, M. D.; Kelly, K. L.; Schatz, G. C.; Van Duyne, R. P. *J. Am. Chem. Soc.* **2001**, *123*, 1471–1482.
(13) AshaRani, P. V.; Mun, G. L. K.; Hande, M. P.; Valiyaveettil, S. *ACS Nano* **2009**, *3*, 279–290.
(14) Schrand, A. M.; Braydich-Stolle, L. K.; Schlager, J. J.; Dai, L.; Hussain, S. M. *Nanotechnology* **2008**, *19*, 23510.
(15) Aroraa, S.; Jaina, J.; Rajwadea, J. M.; Paknikar, K. M. *Toxicol. Appl. Pharmacol.* **2009**, *236*, 310–318.
(16) Daniel, M.-C.; Astruc, D. *Chem. Rev.* **2004**, *104*, 293–346.
(17) Yang, L.; Xing, R.; Shen, Q.; Jiang, K.; Ye, F.; Wang, J.; Ren, Q. *J. Phys. Chem. B* **2006**, *110*, 10534–10539.
(18) Chakraborty, S.; Joshi, P.; Shanker, V.; Ansari, Z. A.; Singh, S. P.; Chakrabarti, P. *Langmuir*, in press.
(19) Drozdowicz-Tomsia, K.; Xie, F.; Goldys, E. M. *J. Phys. Chem. C* **2010**, *114*, 1562–1569.
(20) Peters, T., Jr. *Adv. Protein Chem.* **1985**, *37*, 161–245.
(21) Brown, J. R. *Albumin Structure, Function and Uses*; Rosenoer, V. M., Oratz, M., Rothschild, M. A., Eds.; Pergamon: Oxford, U.K., 1977; Vol. 27.
(22) Peters, T. J. *All About Albumin*; Academic Press: San Diego, CA, 1996.
(23) He, X. M.; Carter, D. C. *Nature* **1992**, *358*, 209–215.
(24) Helms, M. K.; Paterson, V; Bhagavan, N. V.; Jameson, D. M. *FEBS Lett.* **1997**, *408*, 67–70.
(25) Kragh-Hansen, U. *Pharmacol. Rev.* **1981**, *33*, 17.
(26) Sudlow, G.; Birkett, D. J.; Wade, D. N. *Mol. Pharmacol.* **1975**, *11*, 824–832.
(27) Sudlow, G.; Birkett, D. J.; Wade, D. N. *Mol. Pharmacol.* **1976**, *12*, 1052–1061.
(28) Suzuki, Y.; Yokoyama, K. *J. Am. Chem. Soc.* **2005**, *127*, 17799–17802.
(29) Mallick, A.; Halder, B.; Chattopadhyay, N. *J. Phys. Chem. B* **2005**, *109*, 14683–14690.
(30) Das, R.; Guha, D.; Mitra, S.; Kar, S.; Lahiri, S.; Mukherjee, S. *J. Phys. Chem. A* **1997**, *101*, 4042–4047.
(31) Weber, G. *In Light and Life*; McElory, W. D., Glass, B., Eds.; Johns Hopkins: Baltimore, MD, 1961; pp 82−106.
(32) Barreleiro, P. C. A.; Lindman, B. *J. Phys. Chem. B* **2003**, *107*, 6208–6213.
(33) Demchenko, A. P. *Topics in Fluorescence Spectroscopy: Biochemical Applications*; Lakowicz, J. R., Ed.; Plenum: New York, 1992; Vol. 3, p 65.
(34) Cardenas, M.; Schillén, K.; Pebalk, D.; Nylander, T.; Lindman, B. *Biomacromolecules* **2005**, *6*, 832–837.
(35) Haldar, B.; Chakrabarty, A.; Mallick, A.; Mandal, M. C.; Das, P.; Chattopadhyay, N. *Langmuir* **2006**, *22*, 3514–3520.
(36) Mallick, A.; Haldar, B.; Chattopadhyay, N. *J. Phys. Chem. B* **2005**, *109*, 14683–14690.
(37) Chakraborty, A.; Ghosh, S.; Kar, S.; Nath, D. N.; Guchhait, N. *J. Mol. Struct.* **2009**, *917*, 148–157.
(38) Ghosh, S.; Guchhait, N. *ChemPhysChem* **2009**, *10*, 1664–1671.
(39) Mahanta, S.; Singh, R. B.; Guchhait, N. *J. Fluoresc.* **2009**, *19*, 291–303.
(40) Ghosh, S.; Jana, S.; Nath, D. N.; Guchhait, N. *J. Fluoresc.* **2011**, *21*, 365–374.
(41) Lippert, E.; Ludder, W. *Advances in Molecular Spectroscopy*; Pergamon Press: Oxford, 1962.
(42) Grabowski, Z.; Rotkiewicz, K.; Rettig, W. *Chem. Rev.* **2003**, *103*, 3899–4032.
(43) Chakraborty, A.; Kar, S.; Guchhait, N. *J. Photochem. Photobiol., A: Chem.* **2006**, *181*, 246–256.
(44) Chakaraborty, A.; Kar, S.; Nath, D. N.; Guchhait, N. *J. Phys. Chem. A* **2006**, *110*, 12089–12095.
(45) Chakraborty, A.; Kar, S.; Guchhait, N. *Chem. Phys.* **2006**, *324*, 733–741.
(46) Lakowicz, J. R. *Principles of Fluorescence Spectroscopy*; Plenum: New York, 1999.
(47) Schwede, T.; Koop, J.; Guex, N.; Peitsch, M. C. *Nucleic Acid Res.* **2003**, *31*, 3381–3385.
(48) Sugio, S.; Kashima, A.; Mochizuki, S.; Noda, M.; Kobayashi, K. *Protein Eng.* **1999**, *12*, 439–446.
(49) Benyamini, H.; Shulman-Peleg, A.; Wolfson, H. J.; Belgorodsky, B.; Fadeev, L.; Gozin, M. *Bioconjugate Chem.* **2006**, *17*, 378–386.
(50) Frisch, M. J. *Gaussian 03*, Revision B.03; Gaussian, Inc.: Pittsburgh, PA, 2003.
(51) Morris, G. M.; Goodsell, D. S.; Halliday, R. S.; Huey, R.; Hart, W. E.; Belew, R. K.; Olson, A. J. *J. Comput. Chem.* **1998**, *19*, 1639–1662.
(52) Li, J.; Zhu, X.; Yang, C.; Shi, R. *J. Mol. Model.* **2010**, *16*, 789–798.
(53) Neelam, S.; Gokara, M.; Sudhamalla, B.; Amooru, D. G.; Subramanyam, R. *J. Phys. Chem. B* **2010**, *114*, 3005–3012.
(54) Sudhamalla, B.; Gokara, M.; Ahalawat, N.; Amooru, D. G.; Subramanyam, R. *J. Phys. Chem. B* **2010**, *114*, 9054–9062.
(55) Blatt, E.; Husain, A.; Sawyer, W. H. *Biochim. Biophys. Acta* **1986**, *871*, 6–13.
(56) Das, T.; Kumar, A.; Ghosh, P.; Maity, A.; Jaffer, S. S.; Purkayastha, P. *J. Phys. Chem. C* **2010**, *114*, 19635–19640.
(57) Benesi, M. L.; Hildebrand, J. H. *J. Am. Chem. Soc.* **1949**, *71*, 2703–2707.
(58) Valeur, B.; Brochan, J. C. *New Trends in Fluorescence Spectroscopy*; Springer: Berlin, 2001.
(59) Valeur, B. *Molecular Fluorescence: Principles and Applications*; Wiley: New York, 2001.
(60) Davis, D. M.; Birch, D. J. S. *J. Fluoresc.* **1996**, *6*, 23–32.
(61) Gonzalez-Jimenez, V.; Cortijo, M. *J. Protein Chem.* **2002**, *21*, 75–79.
(62) Sarkar, D.; Mahata, A.; Das, P.; Girigoswami, A.; Ghosh, D.; Chattopadhyay, N. *J. Photochem. Photobiol., B* **2009**, *96*, 136–143.
(63) Ravindran, A.; Singh, A.; Raichur, A. M.; Chandrasekaran, N.; Mukherjee, A. *Colloids Surf., B* **2010**, *76*, 32–37.